Damage Identification for Plate Structures Using Transfer Learning Physics-Informed Neural Networks

WEI ZHOU and YONGFENG XU

ABSTRACT

Recently, there has been a growing interest in the development of intelligent label-free structural damage identification methods that utilize physics-informed neural networks (PINNs). However, penalizing the governing equation of training data is computationally time-consuming since the existence of high-order partial derivatives. To address this issue, a damage identification method for isotropic and homogeneous thin plates is proposed in this paper that utilizes transfer learning physics-informed neural networks (TL-PINNs). TL-PINNs are efficient PINNs that solve inverse problems by leveraging transfer learning. Transfer learning is a machine learning technique that leverages knowledge from a source task to enhance performance on a related but different target task. It involves reusing a source model trained on a source task and then fine-tuning it to a target model with a target task. In the proposed method, the source model is trained to minimize the mismatch between training data and its predictions. Then, it is fine-tuned as the target model by minimizing both the mismatch between training data and its predictions as well as residuals that penalize the governing equation of isotropic and homogeneous thin plates. It is resulting in fewer iterations being required in training to penalize the governing equation than those in PINNs, which is time-consuming for high-order partial derivatives using automatic differentiation. Hence, TL-PINNs have a substantial reduction in computational time compared to PINNs for damage identification. A trained TL-PINN from a measured flexural guided wavefield is referred to as a pseudo-pristine model since it can generate a wavefield that approximates that governed by an isotropic and homogeneous thin plate. This unique functionality arises from penalizing the governing equation in the target model and the fact that the governing equation does not consider the existence of the damage. Any local anomalies in the measured wavefield can be isolated by comparing them with the wavefield generated by the pseudo-pristine model and then intensified using the Teager energy operator. An accumulative damage index is formulated, and the damage can be identified within neighborhoods with high index values. The effectiveness of the proposed method is demonstrated through a numerical investigation. A parameter study is also conducted to investigate the robustness of TL-PINNs with different hyper-parameters.

Wei Zhou, PhD Student, Email: zhouw6@mail.uc.edu. Yongfeng Xu, Assistant Professor, Email: xu2yf@uc.edu. Department of Mechanical and Materials Engineering, University of Cincinnati, Cincinnati, OH 45221, USA.

INTRODUCTION

Engineering structures, such as buildings, bridges, and tunnels, are subjected to long-term environmental effects and operational loads that can cause unexpected structural damage. This damage can significantly reduce the service life of these structures, making it important to monitor and identify it in a timely manner. In recent years, the development of graphics processing units and sensing technology has enabled the widespread use of machine learning, particularly deep learning algorithms, in the field of structural damage identification. These algorithms have been applied to various methods of damage identification, including vibration-based methods, guided wavefield-based methods, acoustic emission-based methods, etc. The use of machine learning in structural damage identification has the potential to improve the accuracy and robustness of these methods, enabling more effective monitoring of engineering structures.

The majority of machine learning-based damage identification methods are classified as supervised learning, and as such, the utilization of labeled datasets comprising both training data and corresponding labels regarding the damage is a necessity [1]. In other words, the training process requires vibration data collected for the undamaged structure as well as the data measured under several structural damage scenarios. However, obtaining such datasets can prove to be a challenging task, as they may not be readily available or the process of acquiring them may be time-consuming. This presents a significant limitation in the development and implementation of machine learning-based methods. In recent years, the development of physics-informed neural networks (PINNs) has led to the emergence of label-free damage identification methods based on machine learning [2, 3]. These methods do not rely on labeled datasets, making them a promising alternative for damage identification in practice. Shukla et al. [2] used a PINN for identifying surface-breaking cracks in a metal plate by using measured ultrasonic surface acoustic waves of the metal as the target. The estimated wave velocity field of the metal plate obtained from the PINN served as a damage index. This method demonstrated the feasibility of using PINNs for damage identification in metal structures. Rathod et al. [3] used a trained PINN to identify changes in wave velocity in a rod. The results show that a 50% reduction in Young's modulus in the mid-part of the rod can be represented in the identified wave velocity along the rod, but the sharp variations in wave velocity are not captured.

Transfer learning physics-informed neural networks (TL-PINNs) are efficient PINNs that solve inverse problems by leveraging transfer learning. In the TL-PINNs, a source model is first trained to minimize the mismatch between training data and its predictions. Then, it is fine-tuned as a target model by minimizing both the mismatch between training data and its predictions as well as residuals that penalize the governing equation of training data. It is resulting in fewer iterations being required in training to penalize the governing equation than those in PINNs, which is time-consuming for high-order partial derivatives using automatic differentiation. Hence, TL-PINNs have a substantial reduction in computational time compared to PINNs for damage identification.

In this study, a baseline-free flexural guided wavefield-based damage identification method using TL-PINNs is proposed for plate structures. It assumes a pristine plate structure as an isotropic and homogeneous thin plate and it can be accurately modeled by the Kirchhoff-Love plate theory. A TL-PINN is composed of a source model trained

to minimize the mismatch between predicted and training data, and the source model is fine-tuned as a target model by minimizing the mismatch between training data and its predictions, in addition to residuals that penalize the governing equation of isotropic and homogeneous thin plates. The characteristic parameter in the governing equation, which determines the linear relationship between phase velocity and wavenumber, is estimated during the target model training as an inverse problem. The well-trained target model to obtain a so-called pseudo-pristine plate model. Local anomalies are isolated by differences between the measured wavefield and corresponding predictions by the pseudo-pristine plate model, and they are then intensified by calculating associate two-dimensional Teager energy for each time instant. Finally, an accumulative damage index is formulated using the two-dimensional Teager energy in the time domain. Damage locations and extent can be identified in neighborhoods with high damage index values. The effectiveness of the proposed method is demonstrated through a numerical investigation. A parameter study is also conducted to investigate the robustness of TL-PINNs with different hyper-parameters.

METHODOLOGY

TL-PINNs for isotropic and homogeneous thin plates in inverse problems

Consider an isotropic and homogeneous thin plate governed by the Kirchhoff-Love plate theory, its flexural motion that undergoes free vibrations can be expressed as [4]

$$\nabla^4 u\left(x,y,t\right)+\frac{1}{\alpha^4}\frac{\partial^2 u\left(x,y,t\right)}{\partial t^2}=0 \tag{1}$$

where

$$\alpha=\sqrt[4]{\frac{D}{\rho h}} \tag{2}$$

denotes a characteristic parameter that dictates the linear relationship between the phase velocity and the wavenumber of the plate, in which D, ρ, and h are flexural stiffness, density, and thickness of the plate, respectively.

Consider there is a source domain $\mathcal{D}_S=\left\{x_i^S,y_i^S,t_i^S,u\left(x_i^S,y_i^S,t_i^S\right)\right\}_{i=1}^{N_S}$, and a source task $\mathcal{T}_S$. Besides, there is a target domain, $\mathcal{D}_T=\left\{x_i^T,y_i^T,t_i^T,u\left(x_i^T,y_i^T,t_i^T\right)\right\}_{i=1}^{N_T}$, and a target task $\mathcal{T}_T$. Transfer learning aims to help improve the learning of the target predictive function in $\mathcal{D}_T$ using the knowledge in $\mathcal{D}_S$ and $\mathcal{T}_S$, where $\mathcal{D}_S\neq\mathcal{D}_T$, or $\mathcal{T}_S\neq\mathcal{T}_T$ [5].

For TL-PINNs, a fully connected feed-forward neural network $\mathcal{N}\left(x,y,t;\boldsymbol{\theta}^S\right)$ referred as a source model is first trained on $\mathcal{D}_S$ with the following loss function:

$$\mathcal{L}\left(\boldsymbol{\theta}^S\right)=\frac{1}{N_S}\sum_{i=1}^{N_S}\left\|u\left(x_i^S,y_i^S,t_i^S\right)-u_{\boldsymbol{\theta}^S}\left(x_i^S,y_i^S,t_i^S\right)\right\|^2 \tag{3}$$

where $\|\cdot\|$ denotes an L^2-norm, $u_{\boldsymbol{\theta}^S}\left(x^S,y^S,t^S\right)$ is the output of $\mathcal{N}\left(x,y,t;\boldsymbol{\theta}^S\right)$, and $\mathcal{T}_S$ only considers the mismatch between $u\left(x^S,y^S,t^S\right)$ and $u_{\boldsymbol{\theta}^S}\left(x^S,y^S,t^S\right)$. Leveraging the transfer learning and PINN, $\mathcal{N}\left(x,y,t;\boldsymbol{\theta}^S\right)$ is fine-tuned on $\mathcal{D}_T$ with $\mathcal{T}_T$ as a target

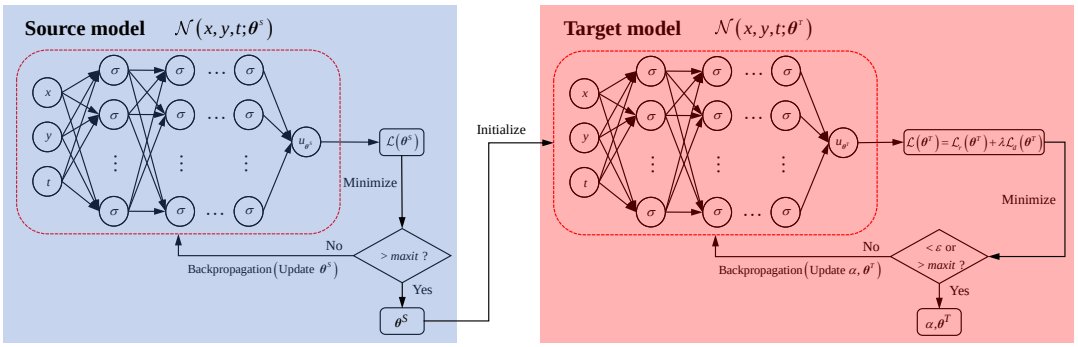

Figure 1. Schematic flowchart of the TL-PINN for an isotropic, homogeneous thin plate to solve the inverse problem. In the convergence criterion shown in the decision box, $maxit$ is the maximum number of iterations and ε is the predefined tolerances of the L-BFGS optimizer.

model $\mathcal{N}\left(x, y, t; \boldsymbol{\theta}^T\right)$, where $\mathcal{D}_T \in \mathcal{D}_S$ and $\mathcal{T}_T$ considers both the mismatch between $u\left(x_i^T, y_i^T, t_i^T\right)$ and $u_{\boldsymbol{\theta}^T}\left(x^T, y^T, t^T\right)$ referred as the output of $\mathcal{N}\left(x, y, t; \boldsymbol{\theta}^T\right)$, and the residual of the governing equation of $u\left(x_i^T, y_i^T, t_i^T\right)$, which is the same task as the PINN. The target model $\mathcal{N}\left(x, y, t; \boldsymbol{\theta}^T\right)$ is trained by minimizing the following composite loss function:

$$\mathcal{L}\left(\boldsymbol{\theta}^T\right) = \mathcal{L}_r\left(\boldsymbol{\theta}^T\right) + \lambda \mathcal{L}_d\left(\boldsymbol{\theta}^T\right) \tag{4}$$

where

$$\mathcal{L}_r\left(\boldsymbol{\theta}^T\right) = \frac{1}{N_T} \sum_{i=1}^{N_T} \left\| \nabla^4 u_{\boldsymbol{\theta}^T}\left(x_i^T, y_i^T, t_i^T\right) + \frac{1}{\alpha^4} \frac{\partial^2 u_{\boldsymbol{\theta}^T}\left(x_i^T, y_i^T, t_i^T\right)}{\partial t^2} \right\|^2 \tag{5}$$

and

$$\mathcal{L}_d\left(\boldsymbol{\theta}^T\right) = \frac{1}{N_T} \sum_{i=1}^{N_T} \left\| u\left(x_i^T, y_i^T, t_i^T\right) - u_{\boldsymbol{\theta}^T}\left(x_i^T, y_i^T, t_i^T\right) \right\|^2 \tag{6}$$

denote the residual loss term and data loss term for $\mathcal{N}\left(x, y, t; \boldsymbol{\theta}^T\right)$, respectively, λ is weighting to adjust the weights of $\mathcal{L}_r\left(\boldsymbol{\theta}^T\right)$ and $\mathcal{L}_d\left(\boldsymbol{\theta}^T\right)$ in $\mathcal{L}\left(\boldsymbol{\theta}^T\right)$. In training the TL-PINN, the value of α is updated at each iteration alongside $\boldsymbol{\theta}^T$. A schematic flowchart for training the TL-PINN is shown in Fig. 1.

Damage identification process

Damage in an isotropic and homogeneous thin plate can lead to local flexural motion anomalies at the site of damage. However, these local anomalies may not be directly discernible from the measured flexural motion, denoted by $u_{med}\left(x, y, t\right)$, when the damage extent is small. In other words, $u_{med}\left(x, y, t\right)$ of such a damaged plate can be highly similar to its pristine counterpart.

Coincidentally, the governing equation of a plate in $\mathcal{N}\left(x, y, t; \boldsymbol{\theta}^T\right)$ corresponds to a pristine one, and it cannot be used to predict the response of a damaged one. Fur-

ther, when $\mathcal{N}\left(x,y,t;\boldsymbol{\theta}^T\right)$ is trained using $u_{med}\left(x,y,t\right)$ of the damaged plate its output can be deemed corresponding to a pristine plate. Hence, when $\mathcal{N}\left(x,y,t;\boldsymbol{\theta}^T\right)$ is well-trained, it can be referred to as a pseudo-pristine plate model. Its predicted output $u_{\boldsymbol{\theta}^T}\left(x,y,t\right)$ can be used to isolate local anomalies on $u_{med}\left(x,y,t\right)$. The differences between $u_{med}\left(x,y,t\right)$ and $u_{\boldsymbol{\theta}^T}\left(x,y,t\right)$ can be obtained:

$$\triangle u\left(x,y,t\right)=u_{med}\left(x,y,t\right)-u_{\boldsymbol{\theta}^T}\left(x,y,t\right) \tag{7}$$

by which the local anomalies in $u_{med}\left(x,y,t\right)$ are isolated to a certain extent when small-extent damage exists. However, non-negligible discrepancies between $u_{med}\left(x,y,t\right)$ and $u_{\boldsymbol{\theta}^T}\left(x,y,t\right)$ away from the damage can mask the local anomalies in $\triangle u\left(x,y,t\right)$. To intensify local anomalies and suppress discrepancies away from the damage, the two-dimensional Teager energy of $\triangle u\left(x,y,t\right)$, denoted by $\mathcal{E}\left(x_i,y_j,t_k\right)$, is calculated for each t_k, and its discrete form can be expressed by [6]

$$\mathcal{E}\left(x_i,y_j,t_k\right)\begin{cases}= & 2\triangle u^2\left(x_i,y_j,t_k\right)-\triangle u\left(x_{i-1},y_j,t_k\right)\triangle u\left(x_{i+1},y_j,t_k\right)\\ & -\triangle u\left(x_i,y_{j-1},t_k\right)\triangle u\left(x_i,y_{j+1},t_k\right),\quad i=2,3,...,N_x-1;\quad j=2,3,...,N_y-1\\ = & 0,\quad i=1,N_x;\quad j=1,N_y\end{cases} \tag{8}$$

where $k=1,2,...,N_t$, in which N_x, N_y and N_t are the number of discrete point of $\triangle u\left(x,y,t\right)$ along x-, y- and t-axes, respectively.

Since $\mathcal{E}\left(x_i,y_j,t_k\right)$ at certain t_k can be insensitive to damage at certain location(s) or it cannot completely indicate its extent [7], there is no guarantee that one or a few $\mathcal{E}\left(x_i,y_j,t_k\right)$ can well identify the damage. Hence, an accumulative damage index is constructed:

$$\mathcal{D}\left(x_i,y_j\right)=\frac{\sum_{k=1}^{N_t}\left|\mathcal{E}\left(x_i,y_j,t_k\right)\right|}{\max\left(\left\{\sum_{k=1}^{N_t}\left|\mathcal{E}\left(x_i,y_j,t_k\right)\right|:i\in\left[1,N_x\right],j\in\left[1,N_y\right]\right\}\right)} \tag{9}$$

where $\max\left(\cdot\right)$ and $\left|\cdot\right|$ denote the maximum and absolute value functions, respectively. It is worth noting that $\mathcal{D}\left(x_i,y_j\right)\in\left[0,1\right]$, and damage can be identified in neighborhoods with high values of $\mathcal{D}\left(x_i,y_j\right)$.

A flowchart summarizing the proposed damage identification method is presented in Fig. 2.

NUMERICAL INVESTIGATION

In this section, a numerical simulation of a plate with damage in the form of two square thickness reduction areas is conducted to investigate the effectiveness of the proposed damage identification method.

Numerical model of an aluminum plate

A free-free-free-free plate with dimensions of 150 mm $\times$ 150 mm and a thickness of 3 mm is simulated using finite element software. The plate is made of aluminum 6061-T6 with the mass density of 2700 kg/m^3, Young's modulus of 68.9 GPa, and Poisson's

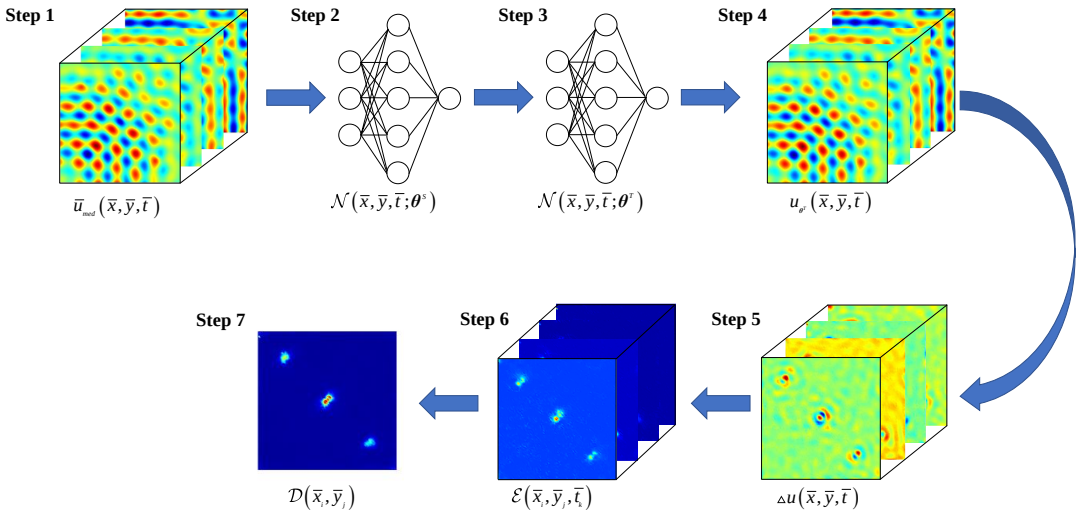

Figure 2. Flowchart of the proposed damage identification method.

ratio of 0.33. Two one-sided square thickness reduction areas with side lengths of 9 mm and depths of 0.3 mm are introduced to the plate and centered at $(34.5, 64.5)$ and $(64.5, 34.5)$ mm.

The finite element model of the plate is constructed with linear eight-node brick (C3D8R) elements. The plate is assumed to have zero initial conditions and is subjected to an excitation force applied to its lower left corner $(0.0, 0.0)$ mm. This force can be described by a five-count wave packet with the magnitude and central frequency of the force being 0.5 N and 30 kHz, respectively [8].

Numerical damage identification

The proposed damage identification method is initially evaluated using a flexural guided wavefield, $u_{med}(x, y, t)$, on a grid consisting of 101×101 measurement points evenly distributed on the plate. The excitation starts at $t = 0$ s and ends at $t = 0.1672$ ms, and the wavefield is then measured with a sampling frequency of 1.25 MHz for $t \in [0.1672, 0.248]$ ms, resulting in a total of 101 snapshots of the free response of the plate. The measured $u_{med}(x, y, t)$ is scaled and the scaled one is denoted by $\bar{u}_{med}(\bar{x}, \bar{y}, \bar{t})$ where $\bar{u}_{med} \in [-1, 1]$, $\bar{x} \in [0, 1]$, $\bar{y} \in [0, 1]$, and $\bar{t} \in [0, 1]$.

Four cases with different hyper-parameters are studied, including in the number of neurons of each hidden layer, activation function, values of N_S, N_T and λ, for constructing a three-layer fully-connected neural network, the hyper-parameters are listed in Table I. The same training dataset is used for training $\mathcal{N}\left(\bar{x}, \bar{y}, \bar{t}; \boldsymbol{\theta}^S\right)$ and $\mathcal{N}\left(\bar{x}, \bar{y}, \bar{t}; \boldsymbol{\theta}^T\right)$ in each case. The source model $\mathcal{N}\left(x, y, t; \boldsymbol{\theta}^S\right)$ is trained by using the Adam optimizer with a learning rate of 0.001 for the number of iterations being $100,000$, and $\mathcal{N}\left(x, y, t; \boldsymbol{\theta}^T\right)$, is trained by using the L-BFGS optimizer with a learning rate of 0.1 for the maximum number of iterations being $50,000$. The tolerances of the L-BFGS optimizer and other parameters of these two optimizers are using default values in PyTorch.

TABLE I. Hyper-parameters of the neural networks in the numerical investigation.

CASE	NUMBER OF NEURONS	ACTIVATION FUNCTION	N_S	N_T	λ
Case 1	50	sine	20,000	20,000	$10,000$
Case 2	50	sine	50,000	50,000	$10,000$
Case 3	50	hyperbolic tangent	20,000	20,000	$10,000$
Case 4	100	sine	20,000	20,000	$10,000$

Numerical verification results

Four pseudo-pristine plate models are obtained after the training of $\mathcal{N}\left(x, y, t; \boldsymbol{\theta}^T\right)$. The predicted wavefields, $u_{\boldsymbol{\theta}^T}\left(\bar{x}, \bar{y}, \bar{t}\right)$, with dimensions same as those of $\bar{u}_{med}\left(\bar{x}, \bar{y}, \bar{t}\right)$, are obtained using pseudo-pristine plate models. The relative L^2 errors $\mathcal{R}$ are used to further examine the relation between $\triangle u\left(\bar{x}, \bar{y}, \bar{t}\right)$ and $\bar{u}_{med}\left(\bar{x}_i, \bar{y}_j, \bar{t}_k\right)$ for each case. The values of $\mathcal{R}$ for cases 1 to 4 are 3.11 %, 2.82 %, 5.35 % and 2.16 %, respectively. It can be observed that the values of $\mathcal{R}$ for the four cases are relative small, indicating that $u_{\boldsymbol{\theta}^T}\left(\bar{x}, \bar{y}, \bar{t}\right)$ well approximates $\bar{u}_{med}\left(\bar{x}_i, \bar{y}_j, \bar{t}_k\right)$ and the difference could derive from the existence of the damage.

The Teager energy $\mathcal{E}\left(\bar{x}_i, \bar{y}_j, \bar{t}_k\right)$ is calculated using Eq. (8) and then $\mathcal{D}\left(\bar{x}_i, \bar{y}_j\right)$ for each case is calculated using Eq. (9), as shown in Fig. 3. It can be seen that high $\mathcal{D}\left(\bar{x}_i, \bar{y}_j\right)$ values exist within the damage areas for these four cases. The location and extent of the damage areas can be accurately identified, despite the different hyper-parameters in each case. To quantitatively evaluate the qualities of the identification results in the four cases, a percentage energy ratio χ is applied [7]. The energy ratio $\chi \in [0, 100\%]$ and a higher χ value indicates a better damage identification results in a lower disturbance from false positive identification results and measurement noise/errors beyond the damaged area(s). The values of χ for cases 1 to 4 are 17.66 %, 19.81 %, 11.91 % and 47.53 %, respectively. It can be observed that the value of χ for each case is negatively correlated with that of $\mathcal{R}$. Specifically, case 4 has the highest value of χ, while case 3 has the lowest value of χ. Hence, the lower values of $\mathcal{R}$ indicate better results for damage identification.

CONCLUDING REMARKS

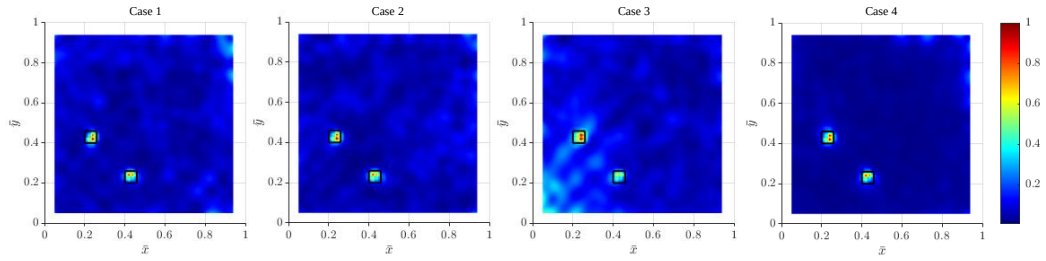

Figure 3. Damage indexes $\mathcal{D}\left(\bar{x}_i, \bar{y}_j\right)$ in the numerical investigation. Edges of the damaged areas are depicted in black lines.

In this study, a novel baseline-free structural damage method for plate structures was developed using TL-PINNs. Pseudo-pristine plate models were constructed using TL-PINNs from measured flexural guided wavefields of damaged plate structures. Local anomalies caused by the existence of damage in flexural guided wavefields are isolated by differences between the measured flexural guided wavefields and corresponding predictions from pseudo-pristine plate models, and they are intensified by the Teager energy at each time instance. The effectiveness of the proposed damage identification method was evaluated through a numerical investigation. It was found that: (1) the proposed method can accurately identify the location and extent of damage, (2) damage can be identified under different hyper-parameters in TL-PINNs, and (3) lower relative L^2 errors between measured flexural guided wavefields and corresponding predictions indicate better damage identification results. In future work, it would be valuable to investigate the proposed method for structures with higher excitation frequencies.

ACKNOWLEDGMENT

The authors are grateful for the financial support from the National Science Foundation through Grant No. CMMI-1762917.

REFERENCES

1. Avci, O., O. Abdeljaber, S. Kiranyaz, M. Hussein, M. Gabbouj, and D. J. Inman. 2021. "A review of vibration-based damage detection in civil structures: From traditional methods to Machine Learning and Deep Learning applications," *Mechanical systems and signal processing*, 147:107077.
2. Shukla, K., P. C. Di Leoni, J. Blackshire, D. Sparkman, and G. E. Karniadakis. 2020. "Physics-informed neural network for ultrasound nondestructive quantification of surface breaking cracks," *Journal of Nondestructive Evaluation*, 39(3):1–20.
3. Rathod, V. and P. Ramuhalli. 2022. "Physics-informed neural networks for identification of material properties using standing waves," in *Nondestructive Characterization and Monitoring of Advanced Materials, Aerospace, Civil Infrastructure, and Transportation XVI*, SPIE, vol. 12047, pp. 179–188.
4. Leamy, M. J. 2016. "Semi-Exact Natural Frequencies for Kirchhoff–Love Plates Using Wave-Based Phase Closure," *Journal of Vibration and Acoustics*, 138(2).
5. Pan, S. J. and Y. Qiang. 2010. "A Survey on Transfer Learning," *IEEE Transactions on Knowledge and Data Engineering*, 22(10):1345–1359.
6. Boudraa, A.-O. and E.-H. S. Diop. 2008. "Image contrast enhancement based on 2D Teager-Kaiser operator," in *2008 15th IEEE International Conference on Image Processing*, IEEE, pp. 3180–3183.
7. Zhou, W., Y. Xu, and J. Kim. 2022. "Baseline-free structural damage identification for plate-like structures based on two-dimensional curvature propagating flexural waves," *Journal of Sound and Vibration*:117098.
8. Zhou, W. and Y. Xu. 2023. "Damage identification for beam-like structures based on proper orthogonal modes of guided wavefields," *Mechanical Systems and Signal Processing*, 189:110052.